DOUBLE STRATFIED FLOW OF NANOFLUID SUBJECT TO TEMPERATURE BASED THERMAL CONDUCTIVITY AND HEAT SOURCE

TASAWAR HAYAT [a,b], IKRAM ULLAH [a] [1], AHMED ALSAEDI [b], MUHAMMAD WAQAS [a]

[a] Department of Mathematics, Quaid-I-Azam University 45320, Islamabad 44000, Pakistan

[b] Nonlinear Analysis and Applied Mathematics (NAAM) Research Group, Department of Mathematics, Faculty of Science, King Abdulaziz University P. O. Box 80203, Jeddah 21589, Saudi Arabia

Abstract: *Stratified hydromagnetic flow of nanomaterial in the zone of stagnation point is addressed. An exponential base space dependent heat source, temperature dependent thermal conductivity and viscous dissipation are accounted. In addition, first order chemical reaction is present. The obtained nonlinear system is computed by employing homotopic procedure. Convergent solutions are obtained. Plots and tabulated values are arranged for interpretation of sundry variables. Clearly temperature and concentration distributions are decayed in presence of stratification. Moreover skin friction and temperature are reduced via wall thickness parameter.*

Keywords: *Exponential space dependent heat source; Double stratification; nanomaterials; variable conductivity.*

Introduction

A stratified fluid is named as the fluid with density fluctuations in the transverse direction. Density difference emerges through various sources such as pressure difference, temperature difference and dissolved phases. The characteristics of thermal and solutal stratifications of hydrogen and oxygen in the lakes and rivers are very significant. Occurrence of wave process and smog in air flow across the mountains are the demonstrations of the influence of stratification in atmosphere. System of thermal storage like solar ponds and heat transfer from thermal sources like condenser of power plant, rivers and seas, heat rejection from environment like lake, geothermal systems, geological transport, thermohydraulic etc. are few examples of applications of stratification. Having such in view, Bansod and Jadhav [1] addressed double stratification in fluid saturated porous medium. Takhar et al. [2] and Chamkha [3] used different methods to explore the free convection flows. They inspected that stratification parameter reduces the temperature and skin friction. Further they found that buoyancy parameter augments the velocity and it diminishes thermal layer thickness. Double stratification in boundary layer flow of nanoliquid by a vertical plate is discussed by Ibrahim and Makinde [4]. Hussain et al. [5] inspected the impact of double stratification in MHD mixed convection flow of Maxwell nanofluid. Hayat et al. [6] presented analysis of mixed convection in doubly stratified flow of Oldroyd-B nanofluid.

Heat transfer liquids have remarkable role in numerous industries such as automotive industry, electronic industries etc. Therefore liquids are frequently utilized as heat transport bearer in the heat transfer apparatus. However the conventional fluids (oil, ethylene glycol, water) are poor heat conducting and usually not fulfilling the heat transfer requirement of recent industrial needs. In order to enhance their conductivity, nanometer sized particles are immersed in base fluids to form nanomaterias. By addition of such particles, thermal heat transfer properties of these liquids can be improved. It is worth to mention here that thermal conductivity, particle size, volume fraction and temperature all participate in advancement of thermal conductivity of nanofluids. The incitement in nanofluid research streams from the heat transfer augmentation in process involving micro-manufacturing, space cooling, microchips in computer processors, fuel cells, nuclear energy, hybridpowered engines, diesel engine oil, air

[1]Corresponding author. Tel.: +92-51 90642172.
email address: ikram020@yahoo.com

refrigerators/air-conditioners and other high energy equipments. The word nanofluid was initially given by Choi [7] which refers to the liquid in which nanometer-sized (less then 100nm) disseminated. He found that addition of very less amount of nanoparticles to traditional heat transfer liquids augmented the thermal conductivity up to two times. This experimental analysis witnessed thermal conductivity enhancement of nanofluid. Buongiorno [8] further constructed a two-phas model to explore the thermal energy transport through nanoliquid. Eastman et al. [9] remarked that a small amount ($<1\%$ volume fraction) of Cu nano-particles or carbon nanotubes immersed in oil or ethylene glycol remarkably boost up the thermal conductivity of a liquid by 50% and 40% respectively. Thus nanomaterials are recognized more significant in micro/nano electromechanical devices, large scale thermal management systems through evaporators, advance cooling systems, industrial cooling applications and heat exchangers. Some other related studies of nanofluids can be seen via refs. [10-22]. Further the magneto nanoliquids (also known as ferrofluid) are special kind of materials which are suspensions of magnetic nanoparticles like magnetite, cobalt ferrite, hematite or some other compound consisting of iron in ordinary base fluid. These particles are more useful in the sense that their physical characteristics are more tunable through the external magnetic field. Also it is worth to noted that in the absence of magnetic field these fluids behave as normal fluids. Magneto nanofluids are profitable to guide the particles up the blood stream to a tumor with magnets. It is because that magnetic nanoparticles are regarded more adhesive to tumor cells when compared with non-malignant cells. Such particles absorb more power than microparticles in alternating current magnetic fields tolerable in humans. Hyperthermia, contrast enhancement in magnetic resonance imaging, magnetic cells separation and delivery are process where magneto nanoliquids involve. In view of such applications many scientists and engineers have interest in investigations of ferrofluids through various aspects. Stretched flow of heated ferrofluid in presence of a magnetic dipole is investigated by Andersson and Valnes [23]. Selimefendigil et al. [24] analyzed forced convection flow of ferrofluid. Rotating flow of magnetite water nanoliquid over a radiative stretching sheet is studied by Mustafa et al. [25]. Hayat et al. [26] examined the partial slip in flow of magnetite-Fe_3O_3 nanoparticles between rotating stretchable disks. MHD three dimensional flow of second grade nanofluid is addressed by Hayat et al. [27]. Sheikholeslami et al. [28] explained external magnetic field effect in force convection flow of nanofluid.

Present work aimed to examined combined effects of double stratification and chemical reaction in stagnation point flow of Williamson nanofluid with variable thermal conductivity. Nonlinear stretching sheet of variable thickness generates the flow. Incompressible electrically conducted fluid is considered with uniform applied magnetic filed. Thermal properties of fluid are examined with viscous dissipation, Brownian motion, exponential based heat source and thermophoresis. Boundary layer approach develops the relevant mathematical formulation. Obtained system of equations is solved through homotopic algorithm [29-42]. Physical quantities of interest are analyzed in detail.

Mathematical development

Here we consider stagnation point flow of Williamson nanoliquid towards nonlinear stretching sheet of variable thickness characterized by $y=\delta(x+b)^{\frac{1-n}{2}}$. Here small δ characterizes that sheet is sufficiently thin. Stretching velocity of sheet is denoted by $U_w = U_0(x+b)^n$. Note that $n=1$ corresponds to case linear stretching. A uniform magnetic field with strength B_0 is applied in transverse direction to the flow. Stratification phenomenon for both heat and mass transfer are addressed. Flow analysis comprises Brownian diffusion and thermophoresis effects. Energy expression is characterize through viscous dissipation and exponential space dependent heat source. Moreover first order chemical reaction are considered. The boundary layer problems satisfy [43-46]:

$$\frac{\partial u}{\partial x}+\frac{\partial v}{\partial y}=0, \tag{1}$$

$$u\frac{\partial u}{\partial x}+v\frac{\partial u}{\partial y}=\nu\frac{\partial^2 u}{\partial y^2}+2\nu\Gamma\frac{\partial u}{\partial y}\frac{\partial^2 u}{\partial y^2}+U_e\frac{\partial U_e}{\partial x}+\frac{\sigma B_0^2}{\rho}(U_e-u), \tag{2}$$

$$u\frac{\partial T}{\partial x}+v\frac{\partial T}{\partial y}=\frac{1}{(\rho c)_f}\frac{\partial}{\partial y}\left(k(T)\frac{\partial^2 T}{\partial y^2}\right)+\frac{(\rho c)_p}{(\rho c)_f}\left(D_B\frac{\partial T}{\partial y}\frac{\partial C}{\partial y}+\frac{D_T}{T_\infty}\left(\frac{\partial T}{\partial y}\right)^2\right) \tag{3}$$

$$+\frac{\mu_0}{(\rho c)_f}\left(\frac{\partial u}{\partial y}\right)^2+\frac{\mu_0}{(\rho c)_f}\Gamma\left(\frac{\partial u}{\partial y}\right)^3+\frac{Q_0(T-T_\infty)}{(\rho c)_f}e^{-n_1\xi},$$

$$u\frac{\partial C}{\partial x}+v\frac{\partial C}{\partial y}=D_B\frac{\partial^2 C}{\partial y^2}+\frac{D_T}{T_\infty}\frac{\partial^2 T}{\partial y^2}-k_1(C_w-C_\infty). \tag{4}$$

$$\left.\begin{aligned} u=U_w=U_0(b+x)^n,\ v=0,\ T=T_w=T_0+d_1(b+x),\\ C=C_w=C_0+d_2(b+x)\quad \text{at } y=\delta(b+x)^{\frac{1-n}{2}},\end{aligned}\right\} \tag{5}$$

$$u\to U_e=U_\infty(x+b)^n,\ T\to T_\infty=T_0+e_1(b+x),\ C\to C_\infty=C_0+e_2(b+x)\text{ as } y\to\infty. \tag{6}$$

In above equations the respective velocity components along $(x,\ y)$ directions are represented by $(u\ ,v)$, $\nu=\frac{\mu_0}{\rho_f}$ the kinematic viscosity, $(b,\ d_1,\ d_2,\ e_1,\ e_2)$ the dimensional constants, Q_0 the heat source parameter, μ_0 the dynamic viscosity, n_1 the exponential index, ρ_f the base liquid density, U_e the free stream velocity, Γ the time constant, n the velocity power index, σ the electrical conductivity, T the temperature, T_0 the reference temperature, $(\rho c)_f$ the heat capacity of liquid, $(\rho c)_p$ nanoparticles effective heat capacity, k_1 chemical reaction rate, D_B the diffusion coefficient, C_0 reference concentration, C the concentration, D_T the coefficient of thermophoretic diffusion, T_∞ and C_∞ the ambient liquid temperature and concentration respectively and U_0 the reference velocity. Consider the variable thermal conductivity in the form [47]:

$$k(T)=k_\infty[1+\varepsilon\frac{T-T_\infty}{\Delta T}], \tag{7}$$

where $\Delta T=T_w-T_0$ and k_∞ the ambient conductivity. With the help of following transformations

$$\left.\begin{aligned} u=U_0\left(x+b\right)^n F'(\eta),\ v=-\sqrt{\left(\tfrac{n+1}{2}\right)\nu U_0\left(x+b\right)^{n-1}}\left[F(\eta)+\eta F'(\eta)\left(\tfrac{n-1}{n+1}\right)\right],\\ \eta=y\sqrt{\left(\tfrac{n+1}{2}\right)\tfrac{U_0\left(x+b\right)^{n-1}}{\nu}},\ \Theta(\eta)=\tfrac{T-T_\infty}{T_w-T_0},\ \Phi(\eta)=\tfrac{C-C_\infty}{C_w-C_0},\end{aligned}\right\} \tag{8}$$

equation (1) is trivially verified while other Eqs. $(2)-(7)$ yield

$$F'''+FF''-\left(\frac{2n}{n+1}\right)F'^2+We\sqrt{\frac{n+1}{2}}F''F'''+\left(\frac{2}{n+1}\right)M^2(\lambda-F')+\left(\frac{2n}{n+1}\right)\lambda^2=0, \tag{9}$$

$$\left.\begin{aligned}\left(1+\varepsilon\Theta\right)\Theta''+\varepsilon\Theta'+\Pr\left(F\Theta'+N_b'\Theta'\Phi'+N_t\Theta'^2-\tfrac{2}{n+1}(\varepsilon_1+\Theta)F'\right)\\ +We\Pr EcF''^3+\Pr EcF''^2+\left(\frac{2}{n+1}\right)\Pr Q\exp(-n_1\xi)\Theta=0,\end{aligned}\right\} \tag{10}$$

$$\Phi''+Sc\left(F\Phi'-\frac{2}{n+1}\varepsilon_2F'\right)+\left(\frac{N_t}{N_b}\right)\Theta''-\left(\frac{2}{n+1}\right)Sc\gamma_1\Phi=0, \tag{11}$$

$$\left.\begin{array}{c} F(\alpha)=\alpha\left(\frac{1-n}{1+n}\right),\ F'(\alpha)=1,\ F'(\infty)\to\lambda, \\ \Theta(\alpha)=1-\varepsilon_1,\ \Theta(\infty)\to 0, \\ \Phi(\alpha)=1-\varepsilon_2,\ \Phi(\infty)\to 0. \end{array}\right\} \tag{12}$$

In above expressions prime signifies derivative with respect to η and $\alpha=\delta\sqrt{\left(\frac{n+1}{2}\right)\frac{U_0}{\nu}}$ designates wall thickness parameter and $\alpha=\eta=\delta\sqrt{\left(\frac{n+1}{2}\right)\frac{U_0}{\nu}}$.

Considering the following expression $F(\eta)=f(\eta-\alpha)=f(\xi)$, $\Theta(\eta)=\theta(\eta-\alpha)=\theta(\xi)$, $\Phi(\eta)=\phi(\eta-\alpha)=\phi(\xi)$ Eqs. $(9)-(12)$ become

$$f'''+ff''-\left(\frac{2n}{n+1}\right)f'^2+We\sqrt{\frac{n+1}{2}}f''f'''+\left(\frac{2}{n+1}\right)M^2(\lambda-f')+\left(\frac{2n}{n+1}\right)\lambda^2=0, \tag{13}$$

$$\left.\begin{array}{l} (1+\varepsilon\theta)\theta''+\varepsilon\theta'+\Pr\left(f\theta'+N_b\theta'\phi'+N_t\theta'^2-\frac{2}{n+1}(\varepsilon_1+\theta)f'\right) \\ +We\Pr Ecf''^3+\Pr Ecf''^2+\left(\frac{2}{n+1}\right)\Pr Q\exp(-n_1\xi)\theta=0, \end{array}\right\} \tag{14}$$

$$\phi''+Sc\left(f\phi'-\frac{2}{n+1}\varepsilon_2 f'\right)+\left(\frac{N_t}{N_b}\right)\theta''-\frac{2}{n+1}Sc\gamma_1\phi=0, \tag{15}$$

$$\left.\begin{array}{c} f(0)=\alpha\left(\frac{1-n}{1+n}\right),\ f'(0)=1,\ f'(\infty)\to\lambda, \\ \theta(0)=1-\varepsilon_1,\ \theta(\infty)\to 0, \\ \phi(0)=1-\varepsilon_2,\ \phi(\infty)\to 0. \end{array}\right\} \tag{16}$$

Here We shows Weissenberg number, Q for exponential space based heat source (ESHS) parameter, Ec for Eckert number, $\Pr$ for Prandtl number, λ for the ratio of velocities, M for magnetic parameter, N_t for thermophoresis parameter, N_b for Brownian motion parameter, γ_1 for chemical reaction, Sc for Schmidt number, ε_1 for thermal stratified parameter, ε for variable thermal conductivity and ε_2 for solutal stratified parameter. The non-dimensional quantities are defined by

$$\left.\begin{array}{c} We=\Gamma\sqrt{\frac{(n+1)U_0^3(x+b)^{3n-1}}{\upsilon}},\ \lambda=\frac{U_\infty}{U_0},\ Ec=\frac{U_w^2}{c_p(T_w-T_0)},\ \Pr=\frac{\mu c_p}{k_\infty}, \\ \varepsilon_1=\frac{e_1}{d_1},\ \varepsilon_2=\frac{e_2}{d_2},\ \gamma_1=\frac{k_1}{U_0}(x+b)^{1-n},\ M^2=\frac{\sigma B_0^2}{\rho U_0(x+b)^{n-1}}, \\ Q=\frac{Q_0}{(\rho c)_f U_0(x+b)^{n-1}},\ Sc=\frac{\nu}{D_B},\ N_b=\frac{(\rho c)_p}{(\rho c)_f}\frac{D_B(C_w-C_0)}{\nu},\ N_t=\frac{(\rho c)_p}{(\rho c)_f}\frac{D_T(T_w-T_0)}{T_\infty\nu}. \end{array}\right\} \tag{17}$$

Expressions of skin friction and rates of heat and mass transfer rates at the surface are

$$C_{fx}=\frac{\tau_{yx}|_{y=\delta(b+x)^{\frac{1-n}{2}}}}{1/2\rho U_w^2}|=\frac{\mu_0\left(\frac{\partial u}{\partial y}+\frac{\Gamma}{2}\left(\frac{\partial u}{\partial y}\right)^2\right)_{y=\delta(x+b)^{\frac{1-n}{2}}}}{\rho U_w^2}, \tag{18}$$

$$Nu_x=\frac{(x+b)q_w|_{y=\delta(b+x)^{\frac{1-n}{2}}}}{k_\infty(T_w-T_\infty)}=-\frac{\left(\frac{\partial T}{\partial y}\right)_{y=\delta(x+b)^{\frac{1-n}{2}}}}{(T_w-T_\infty)}. \tag{19}$$

$$Sh_x = \frac{(x+b)q_m \,|_{y=\delta(b+x)^{\frac{1-n}{2}}}}{D_B(C_w - C_\infty)} = -\frac{\left(\frac{\partial C}{\partial y}\right)_{y=\delta(x+b)^{\frac{1-n}{2}}}}{(C_w - C_\infty)}. \tag{20}$$

In dimensionless form we have

$$\left(\mathrm{Re}_x\right)^{0.5} C_{f_x} = \sqrt{\frac{(n+1)}{2}} f''(0) + \left(\frac{n+1}{4}\right) We f''^2(0), \tag{21}$$

$$\left(\mathrm{Re}_x\right)^{-0.5} Nu_x = -\sqrt{\left(\frac{n+1}{2}\right)} \theta'(0), \tag{22}$$

$$\left(\mathrm{Re}_x\right)^{-0.5} Sh_x = -\sqrt{\left(\frac{n+1}{2}\right)} \phi'(0), \tag{23}$$

where $\mathrm{Re}_x = U_w(b+x)/\nu$ depicts the local Reynolds number.

Homotopic solutions and convergence analysis

The initial approximations (f_0, θ_0, ϕ_0) and linear operators ($\bar{\mathbf{L}}_f$, $\bar{\mathbf{L}}_\theta$, $\bar{\mathbf{L}}_\phi$) are defined as follows

$$\left.\begin{array}{c} f_0(\xi) = \alpha\left(\frac{1-n}{1+n}\right) + (1-\lambda)\left(1 - e^{-\xi}\right) + \lambda\xi, \\ \theta_0(\xi) = (1-\varepsilon_1)e^{-\xi}, \\ \phi_0(\xi) = (1-\varepsilon_2)e^{-\xi}, \end{array}\right\} \tag{24}$$

with

$$\left.\begin{array}{c} \bar{\mathbf{L}}_f\left[\beta_1^{**} + \beta_2^{**}e^{\xi} + \beta_3^{**}e^{-\xi}\right] = 0, \\ \bar{\mathbf{L}}_\theta\left[\beta_4^{**}e^{\xi} + \beta_5^{**}e^{-\xi}\right] = 0, \\ \bar{\mathbf{L}}_\phi\left[\beta_6^{**}e^{\xi} + \beta_7^{**}e^{-\xi}\right] = 0, \end{array}\right\} \tag{25}$$

in which β_j^{**} $(j = 1-7)$ depict the arbitrary constants.

$$(1-\tilde{p})\mathbf{L}_f\left[\hat{f}(\xi,\tilde{p}) - f_0(\xi)\right] = \tilde{p}\hbar_f \mathbf{N}_f[\hat{f}(\xi,\tilde{p})], \tag{26}$$

$$(1-\tilde{p})\mathbf{L}_\theta\left[\hat{\theta}(\xi,\tilde{p}) - \theta_0(\xi)\right] = \tilde{p}\hbar_\theta \mathbf{N}_\theta[\hat{f}(\xi,\tilde{p}), \hat{\theta}(\xi,\tilde{p}), \hat{\phi}(\xi,\tilde{p})], \tag{27}$$

$$(1-\tilde{p})\mathbf{L}_\phi\left[\hat{\phi}(\xi,\tilde{p}) - \phi_0(\xi)\right] = \tilde{p}\hbar_\phi \mathbf{N}_\phi[\hat{f}(\xi,\tilde{p}), \hat{\theta}(\xi,\tilde{p}), \hat{\phi}(\xi,\tilde{p})], \tag{28}$$

$$\left.\begin{array}{c} \hat{f}(0,\tilde{p}) = \alpha\left(\frac{1-n}{1+n}\right), \;\; \hat{f}'(0,\tilde{p}) = 1, \; \hat{f}'(\infty,\tilde{p}) = 0, \\ \hat{\theta}(0,\tilde{p}) = (1-\varepsilon_1), \;\; \hat{\theta}(\infty,\tilde{p}) = 0, \\ \hat{\phi}(0,\tilde{p}) = (1-\varepsilon_1), \;\; \hat{\phi}(\infty,\tilde{p}) = 0, \end{array}\right\} \tag{29}$$

$$\left.\begin{array}{c} \mathbf{N}_f\left[\hat{f}(\xi;\tilde{p})\right] = \frac{\partial^3 \hat{f}}{\partial \xi^3} + \hat{f}\,\frac{\partial^2 \hat{f}}{\partial \xi^2} - \frac{2n}{n+1}\left(\frac{\partial \hat{f}}{\partial \xi}\right)^2 + We\sqrt{\frac{n+1}{2}}\,\frac{\partial^2 \hat{f}}{\partial \xi^2}\,\frac{\partial^3 \hat{f}}{\partial \xi^3} \\ + \frac{2}{n+1} M^2\left(\lambda - \frac{\partial \hat{f}}{\partial \xi}\right) + \frac{2n}{n+1}\lambda^2, \end{array}\right\} \tag{30}$$

$$\left.\begin{aligned}&\mathbf{N}_{\theta}\left[\hat{\theta}(\xi,\tilde{p}),\hat{\phi}(\xi,\tilde{p}),\hat{f}(\xi;\tilde{p})\right]=(1+\varepsilon\hat{\theta})\tfrac{\partial^2\hat{\theta}}{\partial\xi^2}+\varepsilon\hat{\theta}'+\Pr\hat{f}\tfrac{\partial\hat{\theta}}{\partial\xi}+\Pr N_b\tfrac{\partial\hat{\theta}}{\partial\xi}\tfrac{\partial\hat{\phi}}{\partial\xi}\\&+\Pr N_t\left(\tfrac{\partial\hat{\theta}}{\partial\xi}\right)^2-\Pr\tfrac{2}{n+1}(\varepsilon_1+\hat{\theta})\tfrac{\partial\hat{f}}{\partial\xi}+We\Pr Ec\left(\tfrac{\partial\hat{f}}{\partial\xi}\right)^3+\Pr Ec\left(\tfrac{\partial\hat{f}}{\partial\xi}\right)^2+\left(\frac{2}{n+1}\right)\Pr Q\exp(-n_1\xi)\hat{\theta},\end{aligned}\right\}\tag{31}$$

$$\left.\begin{aligned}&\mathbf{N}_{\phi}[\hat{\phi}(\xi,\tilde{p}),\hat{\theta}(\xi,\tilde{p}),\hat{f}(\xi;\tilde{p})]=\tfrac{\partial^2\hat{\phi}}{\partial\xi^2}+Sc\hat{f}\tfrac{\partial\hat{\phi}}{\partial\xi}+\tfrac{N_t}{N_b}\tfrac{\partial^2\hat{\theta}}{\partial\xi^2}\\&-Sc\varepsilon_2\tfrac{2}{n+1}\tfrac{\partial\hat{f}}{\partial\xi}-\tfrac{2}{n+1}Sc\gamma_1\hat{\phi},\end{aligned}\right\}\tag{32}$$

$$\mathbf{L}_f\left[f_m(\xi)-\chi_m f_{m-1}(\xi)\right]=\hbar_f\mathbf{R}_f^m(\xi),\tag{33}$$

$$\mathbf{L}_\theta\left[\theta_m(\xi)-\chi_m\theta_{m-1}(\xi)\right]=\hbar_\theta\mathbf{R}_\theta^m(\xi),\tag{34}$$

$$\mathbf{L}_\phi\left[\phi_m(\xi)-\chi_m\phi_{m-1}(\xi)\right]=\hbar_\phi\mathbf{R}_\phi^m(\xi),\tag{35}$$

$$\left.\begin{aligned}&f_m(0)=f_m'(0)=f_m'(\infty)=0,\ \theta_m(0)=0,\\&\theta_m(\infty)=0,\ \phi_m(0)=0,\ \phi_m(\infty)=0,\end{aligned}\right\}\tag{36}$$

$$\left.\begin{aligned}&\mathbf{R}_f^m(\xi)=f_{m-1}'''(\xi)+\sum_{k=0}^{m-1}f_{m-1-k}f_k''-\tfrac{2n}{n+1}\sum_{k=0}^{m-1}f_{m-1-k}'f_k'+\\&We\sqrt{\tfrac{n+1}{2}}\sum_{k=0}^{m-1}f_{m-1-k}f_k'''\tfrac{2}{n+1}M^2(1-\chi_m)-\tfrac{2}{n+1}M^2f_{m-1}+\tfrac{2n}{n+1}\lambda(1-\chi_m),\end{aligned}\right\}\tag{37}$$

$$\left.\begin{aligned}&\mathbf{R}_\theta^m(\xi)=(1+\varepsilon\theta_{m-1}(\xi))\theta_{m-1}''(\xi)+\varepsilon\theta_{m-1}'(\xi)+\Pr\sum_{k=0}^{m-1}f_{m-1-k}\theta_k'+\Pr N_b\textstyle\sum_{k=0}^{m-1}\phi_{m-1-k}'\theta_k'\\&+\Pr N_t\textstyle\sum_{k=0}^{m-1}\theta_{m-1-k}'\theta_k'-\tfrac{2}{n+1}\Pr\varepsilon_1f_{m-1}'(\xi)-\tfrac{2}{n+1}\Pr\displaystyle\sum_{k=0}^{m-1}f_{m-1-k}\theta_k\\&+We\Pr Ecf_{m-1}''(\xi)\sum_{k=0}^{m-1}f_{m-1-k}''\sum_{l=0}^{k}f_{k-l}''f_l''+\Pr Ec\sum_{k=0}^{m-1}f_{m-1-k}''f_k''+\left(\frac{2}{n+1}\right)\Pr Q\exp(-n_1\xi)\theta_{m-1}(\xi),\end{aligned}\right\}\tag{38}$$

$$\mathbf{R}_\phi^m(\xi)=\phi_{m-1}''(\xi)+Sc\sum_{k=0}^{m-1}f_{m-1-k}\phi_k'+\left(\frac{N_t}{N_b}\right)\theta_{m-1}''(\xi)-\frac{2}{n+1}\varepsilon_2f_{m-1}'(\xi)-\frac{2}{n+1}Sc\gamma_1\phi_{m-1}(\xi),\tag{39}$$

$$\chi_m=\begin{cases}0,\ m\le 1,\\1,\ m>1.\end{cases}\tag{40}$$

The general solutions $(f_m(\xi),\ \theta_m(\xi),\ \phi_m(\xi))$ of the governing in the form of special solutions $(f_m^*(\xi),\ \theta_m^*(\xi),\ \phi_m^*(\xi))$ are:

$$f_m(\xi)=f_m^*(\xi)+\beta_1^{**}+\beta_2^{**}e^{\xi}+\beta_3^{**}e^{-\xi},\tag{41}$$

$$\theta_m(\xi)=\theta_m^*(\xi)+\beta_4^{**}e^{\xi}+\beta_5^{**}e^{-\xi},\tag{42}$$

$$\phi_m(\xi)=\phi_m^*(\xi)+\beta_6^{**}e^{\xi}+\beta_7^{**}e^{-\xi},\tag{43}$$

Obviously homotopic procedure for local similar solutions involves embedding variables which gives the flexibility to enlarge the convergence region. Thus h-curves are displayed which enable us to find the acceptable values of $\hbar_f$, $\hbar_\theta$ and $\hbar_\phi$ (Figs. 1 & 2). Allowed ranges of $\hbar_f$, $\hbar_\theta$ and $\hbar_\phi$ are $-1.10\le\hbar_f\le-2.00]$, $[-0.40\le\hbar_\theta\le-1.40]$ and $[-0.50\ \le\hbar_\phi\le-1.63]$. Further HAM solutions converge when $\hbar_f = -5.0 = \hbar_\theta$ and $\hbar_\phi = -0.6$ (see Table 1).

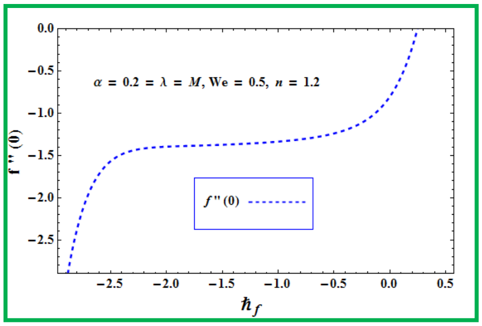

Figure 1: $\hbar-$curves for $f(\xi)$.

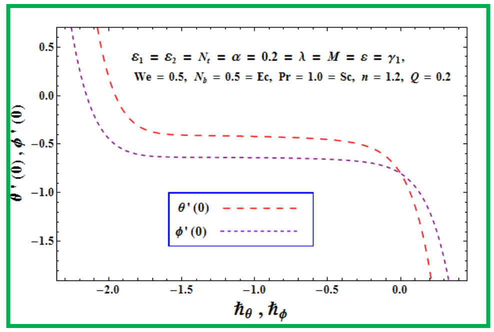

Figure 2: $\hbar-$curves for $\theta(\xi)$ and $\varphi(\xi)$.

Table 1: Convergence of solutions when $Ec = N_b = 0.5 = We$
$Q = M = \alpha = 0.2 = n = \lambda = \varepsilon = \varepsilon_1 = \varepsilon_2 = N_t = \gamma_1$ and $\Pr = 1.0 = Sc$.

Order of estimations	$-f''(0)$	$\theta'(0)$	$\phi'(0)$
1	0.88582	0.88582	0.75752
10	1.21754	1.21754	0.65816
15	1.28024	1.28024	0.64700
20	1.32201	1.32201	0.64057
25	1.33218	1.33218	0.63923
30	1.33218	1.33218	0.63912
40	1.33218	1.33218	0.63911

Discussion

The transformed problems defined in eqs.(13)-(16) is solved analytically via homotopic technique. Influence of some sundry variables like Weissenberg number (We), velocities ratio parameter (λ), (ESHS) parameter (Q), magnetic parameter (M), variable thermal conductivity parameter (ε), velocity power index (n), Prandtl number $(\Pr)$, thermophoresis parameter (N_t), Eckert number (Ec), Brownian motion parameter (N_b), thermal stratified parameter (ε_1), solutal stratified parameter (ε_2), Schmidt number (Sc), chemical reaction (γ_1) and wall thickness parameter (α) velocity, temperature, concentration, local Nusselt and Sherwood numbers. For such intention Figs. $3-22$ have been interperted. The role of wall thickness parameter α on $f'(\xi)$ is depicted in Figs. 3 and 4. It is noted here that $f'(\xi)$ near the plate decays as α increases for $n>1$ (see Fig. 3) and opposite trend is seen for $n<1$ (see Fig. 4). Graphical presentation for velocity field as a function of n is elucidated through Fig. 5. It appears that larger n cause to enhanced the stretching velocity which accelerates the fluid motion and consequently the fluid velocity increases. Thickness of momentum layer becomes thin as n increases. Impact of We on $f'(\xi)$ is presented in Fig. 6. In physical sense, We increases the fluid thickness and consequently velocity profile $f'(\xi)$ decays. Behavior of λ on $f'(\xi)$ is disclosed via Fig. 7. It is examined that velocity enhances with increment in λ. Thickness of momentum layer increases for $A<1$. Here stretching velocity dominates the free stream velocity. Variation in $\theta(\xi)$ via ε is examined in Fig. 8. Here increment in ε boosts up liquid temperature significantly. Fig. 9 is portrayed to see the changes in N_t for $\theta(\xi)$. It is noticed that when we strengthen N_t from $N_t = 0.2$ to $N_t = 1.0$, it sharply rises $\theta(\xi)$ and thermal layer thickness. More precisely we can say that thermophoresis force has the property that nanoparticles near the hot surface are being pushed towards the cold region at the boundary. Thus in presence of N_t one can expects thermal layer to become thicker. Feature of $\Pr$ on $\theta(\xi)$ is portrayed in Fig. 10. Reduction in $\theta(\xi)$ is noticed for higher $\Pr$. By increasing $\Pr$ the thermal diffusivity diminishes because heat rapidly transfers that causes a drop in temperature distribution. Analysis for behavior of Ec is depicted in Fig. 11. It is concluded that $\theta(\xi)$ is an increasing function of Ec. Physically frictional heating is associated with higher Ec thus have $\theta(\xi)$ increases. Effects of wall thickness parameter α on $\theta(\xi)$ is illustrated in Fig. 12. It is concluded that $\theta(\xi)$ is decaying function of α. In fact significant amount of heat transferred from surface to fluid when α is incriminated. Fig. 13 displays characteristics of ε_1 on $\theta(\xi)$. Clearly $\theta(\xi)$ reduces for larger thermal stratification parameter. It is because of the fact that temperature difference slowly decays between the sheet and ambient liquid. Temperature is an increasing function of Q (see Fig. 14). Influence of N_t on $\phi(\xi)$ is drawn in Fig. 15. Here $\phi(\xi)$ is higher for N_t. Salient feature of N_b on nanoparticles concentration $\phi(\xi)$ is declared in Fig. 16. For larger N_b a decreasing trend of $\phi(\xi)$ is noticed. Concentration distribution is reduced via Sc (see Fig. 17). Fig. 18 shows effects of ε_2 on $\phi(\xi)$. It is reveled that $\phi(\xi)$ decreases via ε_2. This is due to small difference of surface and ambient concentration. Role of γ_1 on $\phi(\xi)$ is captured in Fig. 19. Clearly stronger γ_1 lead to reduce $\phi(\xi)$ and solutal boundary layer thickness. Fig. 20 shows N_b and N_t variations for Nusselt number. It is found that heat transfer rate diminishes for larger N_b while it increases via N_t. Fig. 21 shows that Nusselt number for higher M while reverse is seen for larger n. It is noticed that Nusselt number increases for. Variations of n and Sc on Sherwood number ($Sh_x \mathrm{Re}_x^{-0.5}$) are portrayed in Fig. 22. Clearly $Sh_x \mathrm{Re}_x^{-0.5}$ boosts up for higher values of Sc and n. Numerical data of $-f''(0)$, $-\theta'(0)$ and $-\phi'(0)$ for various order of estimations are demonstrated in Table 1 when $Q = M = \alpha = 0.2 = n = \lambda = \varepsilon = \varepsilon_1 = \varepsilon_2 = N_t = \gamma_1$, $Ec = N_b = 0.5 = We$, $\Pr = 1.0 = Sc$, and $\hbar_f = \hbar_\theta = -0.4 = \hbar_\phi$. It is depicted that 30^{th} order of estimations are enough for convergence of homotopic solutions. Numerical results of skin friction $-(\mathrm{Re})^{1/2} C_{fx}$ for various values of λ, We, M, n and α are presented in Table 2. Here skin friction is enhanced via λ, M, We and α.

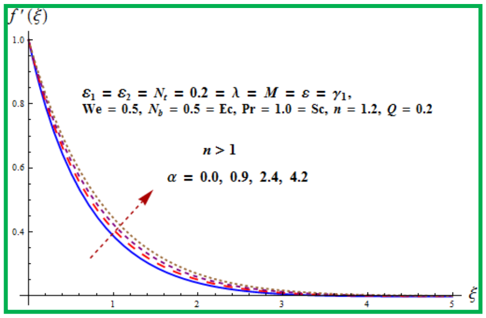

Figure 3: Impact of $f'(\xi)$ via α $(n>1)$.

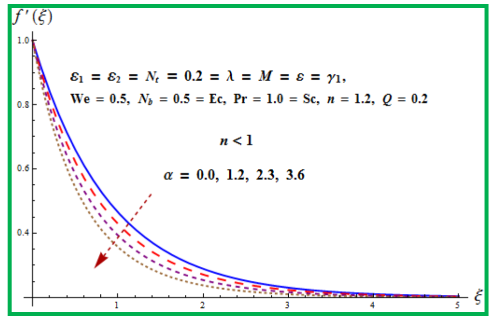

Figure 4: Impact of $f'(\xi)$ via α $(n<1)$.

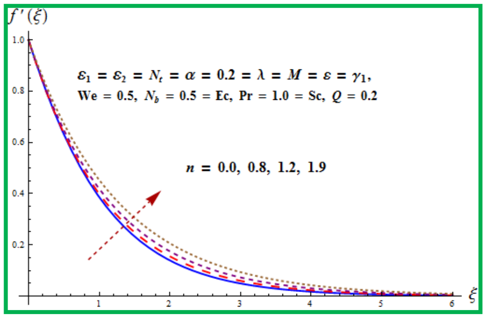

Figure 5: Impact of $f'(\xi)$ via n.

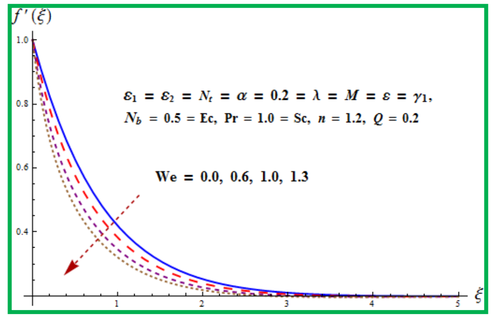

Figure 6: Impact of $f'(\xi)$ via We.

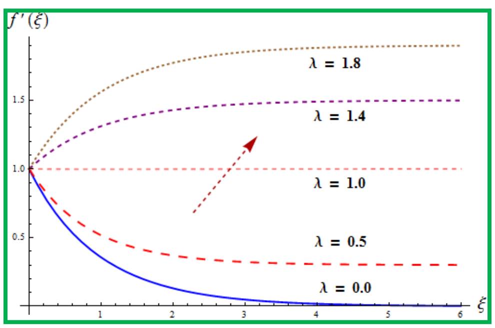

Figure 7: Impact of $f'(\xi)$ via λ.

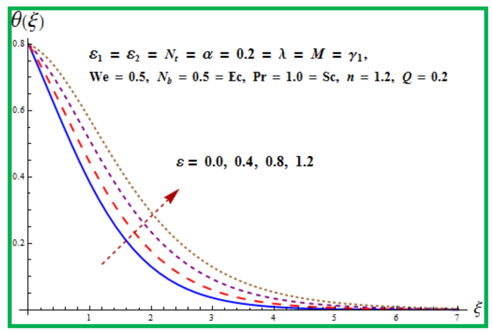

Figure 8: Impact of $\theta(\xi)$ via ε.

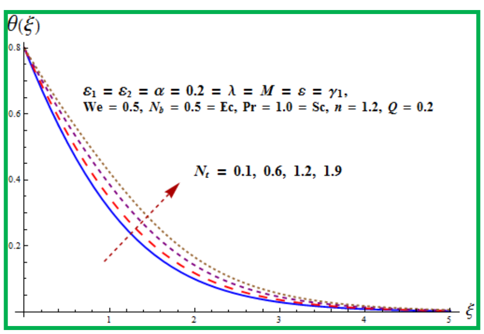

Figure 9: Impact of $\theta(\xi)$ via N_t.

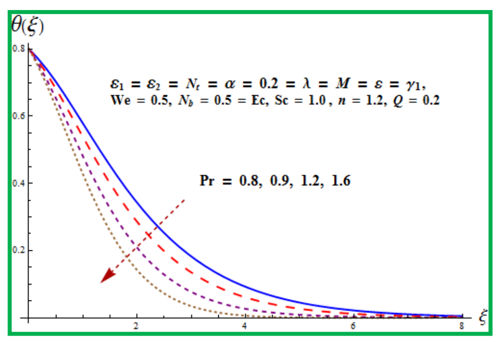

Figure 10: Impact of $\theta(\xi)$ via Pr.

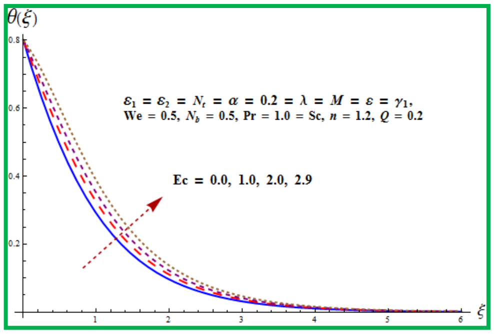

Figure 11: Impact of $\theta(\xi)$ via Ec.

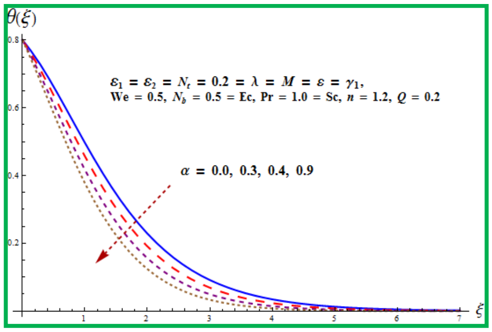

Figure 12: Impact of $\theta(\xi)$ via α.

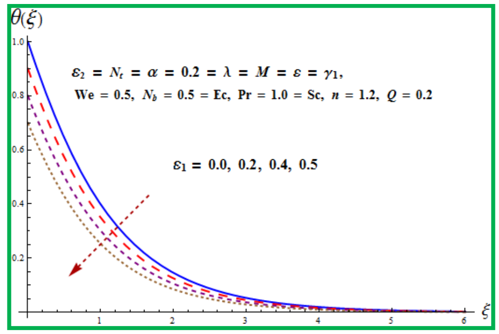

Figure 13: Impact of $\theta(\xi)$ via ε_1.

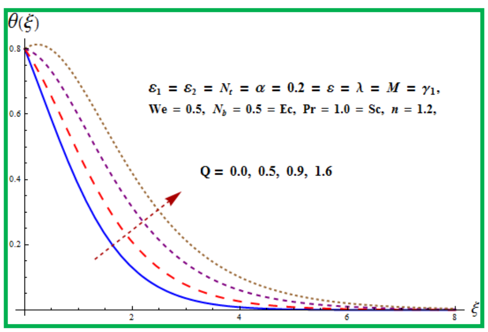

Figure 14: Impact of $\theta(\xi)$ via Q.

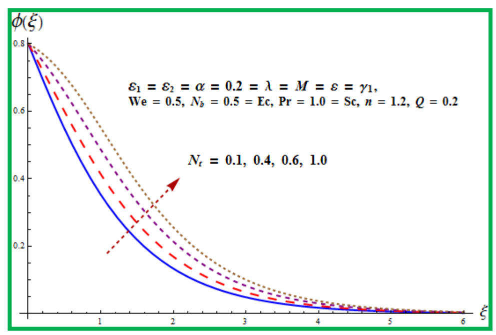

Figure 15: Impact of $\phi(\xi)$ via N_t.

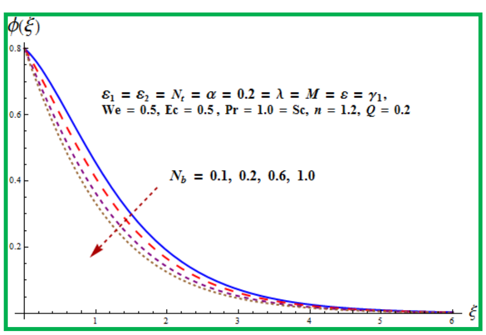

Figure 16: Impact of $\phi(\xi)$ via N_b.

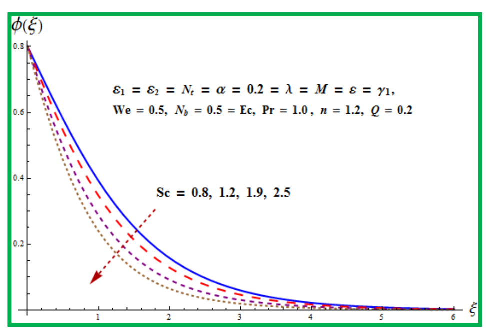

Figure 17: Impact of $\phi(\xi)$ via Sc.

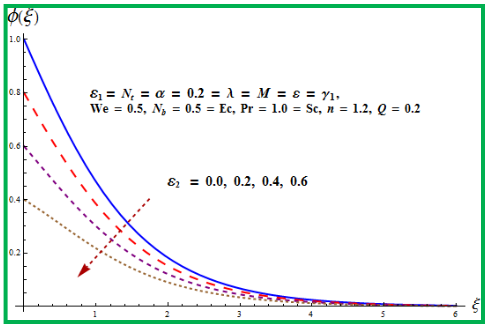

Figure 18: Impact of $\phi(\xi)$ via ε_2.

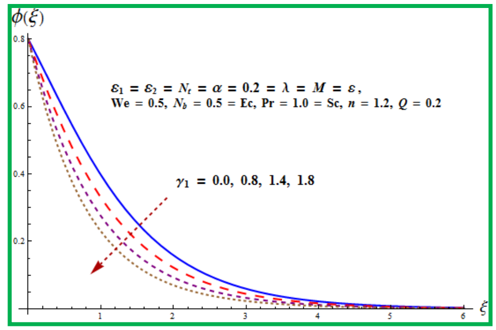

Figure 19: Impact of $\phi(\xi)$ via γ_1.

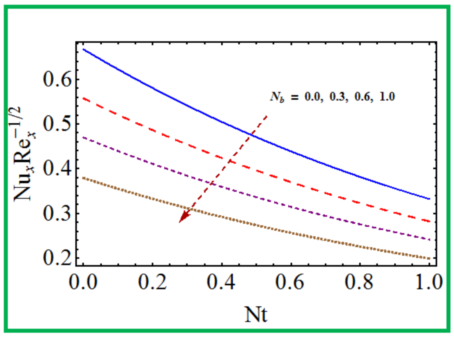

Figure 20: Impact of N_b via N_t on $Nu_x \mathrm{Re}_x^{-0.5}$.

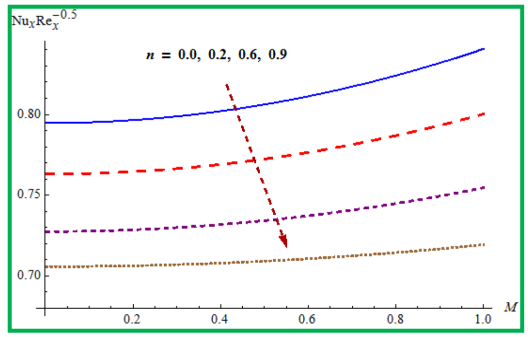

Figure 21: Impact of n via M on $Nu_x \mathrm{Re}_x^{-0.5}$.

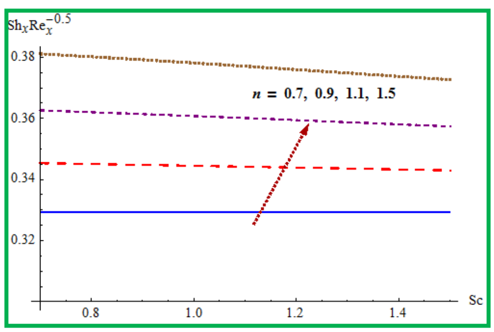

Figure 22: Impact of n via Sc on $Sh_x \mathrm{Re}_x^{-0.5}$.

Table 2: Computation for numerical data of surface drag force $-(\mathrm{Re})^{0.5} C_{fx}$ for distinct values of We, M, n, λ and α.

Parameters (fixed values)	Parameters		$-\mathrm{Re}^{\frac{1}{2}} C_{fx}$
$Q=\alpha=0.2=n=\lambda=\varepsilon=\varepsilon_1=\varepsilon_2=N_t=\gamma_1,$	M	0.0	0.930131
$Ec=N_b=0.5=We$, $\Pr=1.0=Sc.$		0.3	0.946343
		0.6	0.983631
$Q=M=\alpha=0.2=n=\lambda=\varepsilon=\varepsilon_1=\varepsilon_2=N_t=\gamma_1,$	We	0.0	1.94118
$Ec=N_b=0.5$, $\Pr=1.0=Sc.$		0.4	1.245294
		0.8	0.478471
$Q=M=\alpha=0.2=\lambda=\varepsilon=\varepsilon_1=\varepsilon_2=N_t=\gamma_1,$	n	0.5	0.865803
$Ec=N_b=0.5=We$, $\Pr=1.0=Sc.$		1.0	0.961150
		1.5	0.975210
$Q=M=0.2=n=\lambda=\varepsilon=\varepsilon_1=\varepsilon_2=N_t=\gamma_1,$	α	0.2	0.951138
$Ec=N_b=0.5=We$, $\Pr=1.0=Sc.$		0.6	0.938785
		0.8	0.928758
$Q=M=\alpha=0.2=n=\varepsilon=\varepsilon_1=\varepsilon_2=N_t=\gamma_1,$	λ	0.2	0.930158
$Ec=N_b=0.5=We$, $\Pr=1.0=Sc.$		0.5	0.887362
		0.8	0.125043

Concluding remarks

Main observations of carried out analysis are outlined below:

- Wall thickness parameter α decreases both velocity and temperature.
- Increment in We reduces the velocity field.
- Both ε_1 and ε_2 have similar effects on temperature and concentration.
- Higher values of ε augment fluid temperature.
- Temperature and concentration show increasing behavior when N_t is enhanced.
- Skin friction reduces for higher n.
- Features of N_t and N_b on Nusselt number are quite reverse.

Nomenclature

u, v– velocity components	ε – variable thermal conductivity parameter
x, y – Cartesian coordinates	b, d_1, d_2, e_1, e_2 – dimensional constants
T_w, T – wall and liquid temperatures	n – velocity power index
D_B, D_T – coefficients of Brownian and themophoretic diffusion	n_1 – exponential index
C_{fx} – skin friction	$(\rho c)_p$ – heat capacity of liquid
μ_0 – dynamic viscosity	$(\rho c)_f$ – nanoparticles effective capacity

U_e – free stream velocity	ϕ, Φ – dimensionless concentration
σ – electrical conductivity	ρ – fluid density
U_w, U_0 – stretching and reference velocities	k_∞ – ambient thermal conductivity
Re_x – local Reynolds number	θ, Θ – dimensionless temperatures
C, C_w – nanoparticles and wall concentrations	N_t – Thermopherasis parameter
C_∞, C_0 – ambient and reference concentrations	N_b – Brownian motion parameter
Q_0 –heat source parameter	Pr – Prandtl number
Γ – time constant	α – wall thickness parameter
T_∞, T_0 –ambient and reference temperatures	We – Weissenberg number
f', F – dimensionless velocities	M – magnetic parameter
μ_0 – dynamic viscosity	λ – ratio of velocities
ν – kinematic viscosity	Q – ESHS parameter
δ – small parameter regarding the surface sufficiently thin	$\varepsilon_1, \varepsilon_2$ – thermal and solutal stratified parameters
k_1 – chemical reaction rate	γ_1 – chemical reaction parameter
Sc – Schmidt number	Ec – Eckert number
Sh_x – Sherwood number	Nu_x – Nusselt number

References

[1] Bansod, V., Jadhav, R., Effect of double stratification on mixed convection heat and mass transfer from a vertical surface in a fluid-saturated porous medium, *Heat Transfer Asian Research, 39* (2010), pp. 378-395

[2] Takhar, H. S., Chamkha, A. J., Nath, G., Natural convection flow from a continously moving vertical surface immersed in a thermally stratified medium, *Heat Mass transfer, 38* (2001), pp. 17-24

[3] Chamkha, A. J., Hydromahnetic natural convection from an isothermal inclined surface adjacent to a thermally stratified porous medium, *International Journal of Engineering Science*, *35* (1997), pp. 975-986

[4] Ibrahim, W., Makinde, O. D., The effect of double stratification on boundary-layer flow and heat transfer of nanofluid over a vertical plate, *Computers and Fluids, 86* (2013), pp. 433-441

[5] Hussain, T., Hussain, S., Hayat, T., Impact of double stratification and magnetic field in mixed convective radiative flow of Maxwell nanofluid, *Journal of Molecular Liquids, 220* (2016), pp. 870-878

[6] Hayat, T., Ullah, I., Muhammad, T., Alsaedi, A., Thermal and solutal stratification in mixed convection three-dimensional flow of an Oldroyd-B nanofluid, *Results in Physics*, *7* (2017), pp. 3797-3805

[7] Choi, S. U. S., Enhancing thermal conductivity of fluids with nanoparticles, *USA, ASME, FED 231/MD, 66* (1995), pp. 99-105.

[8] Buongiorno, J., Convective transport in nanofluids, *Journal of Heat Transfer*, 128 (2006), pp. 240-250

[9] Eastman, J. A., Choi, S. U. S., Li, S., Yu, W., Thompson, L. J., Anomalously increased efffective

thermal conductivity of ethylene glycol-based nanofluids containing copper nanoparticles, *Applied Physics Letters*, *78* (2001), pp. 718-720
[10] Turkyilmazoglu, M., Exact analytical solutions for heat and mass transfer of MHD slip flow in nanofluids, *Chemical Engineering Science, 84* (2012), pp. 182-187
[11] Sheikholeslami, M., Hayat, T. Alsaedi, A., MHD free convection of Al_2O_3 -water nanofluid considering thermal radiation: A numerical study, *International Journal of Heat and Mass Transfer, 96* (2016), pp. 513-524.
[12] Hsiao, K. L., Stagnation electrical, MHD nanofluid mixed convection with slip boundary on a stretching sheet, *Applied Thermal Engineering, 98* (2016), pp. 850-861.
[13] Hayat, T., Ullah, I., Alsaedi, A., Ahmad, B., Modeling tangent hyperbolic nanoliquid flow with heat and mass flux conditions, *The European Physical Journal Plus, 132* (2017), pp. 112.
[14] Zhang, C., Zheng, L., Zhang, X., Chen, G., MHD flow and radiation heat transfer of nanofluids in porous media with variable surface heat flux and chemical reaction, *Applied Mathematical Modelling, 39* (2015), pp. 165-181
[15] Hayat, T., Ullah, I., Muhammad, T., Alsaedi, A., Shehzad, S. A., Three-dimensional flow of Powell-Eyring nanofluid with heat and mass flux boundary conditions, *Chines Physics B, 25* (2016), pp. 074701
[16] Malvandi, A., Ganji , D. D., Pop, I., Laminar filmwise condensation of nanofluids over a vertical plate considering nanoparticles migration, *Applied Thermal Engineeing*, *100* (2016), pp. 979-986
[17] Hayat, T., Ullah, I., Alsaedi, A., Waqas, M., Ahmad, B., Three-dimensional mixed convection flow of Sisko nanoliquid, *International Journal of Mechanical Sciences, 133* (2017), pp. 273-282
[18] Hsiao, K. L., To promote radiation electrical MHD activation energy thermal extrusion manufacturing system efficiency by using Carreau-Nanofluid with parameters control method, *Energy, 130* (2017), pp. 486e499
[19] Hayat, T., Ullah, I., Alsaedi, A., Farooq, M., MHD flow of Powell-Eyring nanofluid over a non-linear stretching sheet with variable thickness, *Results in Physics, 7* (2017), pp. 189-196
[20] Hsiao, K. L., Micropolar nanofluid flow with MHD and viscous dissipation effects towards a stretching sheet with multimedia feature, *International Journal of Heat and Mass Transfer, 112* (2017), pp. 983-990
[21] Hayat, T., Ullah, I., Alsaedi, A., Asghar, S., Flow of magneto Williamson nanoliquid towards stretching sheet with variable thickness and double stratification, *Radiation Physics and Chemistry*, (2018), doi.org/10.1016/j.radphyschem.2018.07.006
[22] Ullah, I., Waqas, M., Hayat, T., Alsaedi A., Khan, M. I., Thermally radiated squeezed flow of magneto-nanofluid between two parallel disks with chemical reaction, *Journal of Thermal Analysis and Calorimetry,* (2018) Doi.org/10.1007/s10973-018-7482-6
[23] Andersson, H. I., Valnes, O. A., Flow of a heated ferrofluid over a stretching sheet in the presence of a magnetic dipole, *Acta Mechanica*, *128* (1998), pp. 39-47
[24] Selimefendigil, F., Oztop, H. F., Al-Saleem, K., Effect of rotating cylender in forced convection of ferrofluid over a backward facing step, *International Journal of Heat and Mass Transfer, 372* (2014), pp. 122-133
[25] Mustafa, M., Mushtaq, A., Hayat, T., Alsaedi, A., Rotating flow of magnetite-water nanofluid over a stretching surface inspired by non-linear thermal radiation, *Plos One, 11* (2016), pp. e0149304
[26] Hayat T., Qayyum, S., Imtiaz, M., Alzahrani F., Alsaedi, A., Partial slip effect in flow of magnetite-Fe_3O_3 nanoparticles between rotating stretchable disk, *Journal of Magnetism and Magnetic Materials*, *423* (2016), pp. 39-48
[27] Hayat, T., Ullah, I., Muhammad, T., Alsaedi, A., Magnetohydrodynamic (MHD) three-dimensional flow of second grade nanofluid by a convectively heated exponentially stretching surface, *Journal of Molecular Liquids, 220* (2016), pp. 1004-1012
[28] Sheikholeslami, M., Hayat T., Alsaedi, A., Numerical simulation of nanofluid forced convection

heat transfer improvement in existence of magnetic field using lattice Boltzmann method, *International Journal of Heat and Mass Transfer, 108* (2017), pp. 1870-1883

[29] Liao, S. J., On the homotopy analysis method for nonlinear problems, *Applied Mathematics and Computation, 147* (2004), pp. 499-513

[30] Hayat, T., Ali, S., Awais, M., Alsaedi, A., Joule heating effects in MHD flow of Burgers' fluid, *Heat Transfer Research, 47* (2016), pp. 1083-1092

[31] Abbasbandy, S., Hayat, T., Alsaedi, A., Rashidi, M. M., Numerical and analytical solutions for Falkner-Skan flow of MHD Oldroyd-B fluid, *International Journal of Numerical Methods Heat Fluid Flow, 24* (2014), pp. 390-401

[32] Hayat, T., Ali, S., Farooq, M. A., Alsaedi, A., On comparison of series and numerical solutions for flow of Eyring-Powell fluid with Newtonian heating and internal heat generation/absorption, *PloS one, 10* (2015), pp. e0129613

[33] Zhn, J., Yang, D., Zaheng, L., Zhang, X., Effects of second order velocity slip and nanoparticles migration on flow of Buongiorno nanofluid, *Applied Mathematical Letters., 52* (2016), pp. 183-191

[34] Turkyilmazoglu, M., An effective approach for evaluation of the optimal convergence control parameter in the homotopy analysis method, *Filomat, 30* (2016), pp. 1633-1650

[35] Hayat, T., Ullah, I., Muhammad, T., Alsaedi, A., Radiative three-dimensional flow with Soret and Dufour effects, *International Journal of Mechanical Sciences, 133* (2017), pp. 829-837

[36] Hayat, T., Ali, S., Alsaedi, A., Alsulami, H. H., Influence of thermal radiation and Joule heating in the Eyring-Powell fluid flow with the Soret and Dufour effects, *Journal of Applied Mechanics and Technical Physics, 57* (2016), pp. 1051-1060

[37] Hayat, T., Ullah, I., Muhammad, T., Alsaedi, A., A revised model for stretched flow of third grade fluid subject to magneto nanoparticles and convective condition, *Journal of Molecular Liquids, 230* (2017), pp. 608-615

[38] Farooq, A., Ali, R., Benim, A. C., Soret and Dufour effects on three dimensional Oldroyd-B fluid, *Physica A, 503* (2018), pp. 345-354

[39] Hayat, T., Ullah, I., Alsaedi, A., Ahmad, B., Radiative flow of Carreau liquid in presence of Newtonian heating and chemical reaction, *Results Physics, 7* (2017), pp. 715-722

[40] Hayat, T., Ullah, I., Ahmed, B., Alsaedi, A., MHD mixed convection flow of third grade liquid subject to non-linear thermal radiation and convective condition, *Results Physics, 7* (2017), pp. 2804-2811

[41] Rashidi, M. M., Ashraf, M., Rostami, B., Rastegari, M. T., Bashir, S., Mixed convection boundary layer flow of micro polar fluid towards a heated shrinking sheet by homotopy analysis method, *Thermal science, 20* (2016), pp. 21-34

[42] S. Ahmad, Khan, M. I., Khan, M. W. A., Tufail, A., Hayat, T., Ahmed. A., Impact of arrhenius activation energy in viscoelastic nanomaterial flow subject to binary chemical reaction and nonlinear mixed convection, *Thermal Science,* (2018) pp. 212-212

[43] Zaigham Zia, Q. M., Ullah, I., Waqas, M., Alsaedi, A., Hayat, T., Cross diffusion and exponential space dependent heat source impacts in radiated three-dimensional (3D) flow of Casson fluid by heated surface, *Results in Physics, 8* (2018), pp. 1275-1282

[44] Hsiao, K. L., Combined electrical MHD heat transfer thermal extrusion system using Maxwell fluid with radiative and viscous dissipation effects, *Applied Thermal Engineering, 112* (2017), pp.1281-1288

[45] Hayat, T., Ullah, I., Alsaedi A., and Ahmad, B., Simultaneous effects of non-linear mixed convection and radiative flow due to Riga-plate with double stratification, *Journal of Heat Transfer, 140* (2018), pp. 102008

[46] Reddy C, S., Naikoti, K., Rashidi, M. M., MHD flow and heat transfer characteristics of Williamson nanofluid over a stretching sheet with variable thickness and variable thermal conductivity, *Transactions of A. Razmadze Mathematical Institute*, *171* (2017), pp. 195-211
[47] Hayat, T., Ullah, I., Waqas, M., Alsaedi, A., Flow of chemically reactive magneto Cross nanoliquid with temperature-dependent conductivity, *Applied Nanosciences*, (2018), doi.org/10.1007/s13204-018-0813-x.